Effect of scour on the fatigue life of offshore wind turbines and its prevention through passive structural control

Yu Cao[1], Ningyu Wu[2], Jigang Yang[2], Chao Chen[1,3*], Ronghua Zhu[3,4*], Xugang Hua[1],

[1] Key Laboratory for Bridge and Wind Engineering of Hunan Province, College of Civil Engineering, Hunan University, Changsha, China

[2] Hebei Construction Investment Offshore Wind Power Co., Ltd., Tangshan, China

[3] Yangjiang Offshore Wind Laboratory, Yangjiang, China

[4] Ocean College, Zhejiang University, Hangzhou, China

*Corresponding author: steinchen@hnu.edu.cn, zhu.richard@zju.edu.cn

Abstract

Offshore wind turbine (OWT) support structures are exposed to the risk of fatigue damage and scour, and this risk can be effectively mitigated by installing structural control devices such as tuned mass dampers (TMDs). However, time-varying scour altering OWTs' dynamic characteristics has an impact on the TMD design and fatigue life, which was rarely studied before. In this paper, a simplified modal model is used to investigate the influence of scour and a TMD on the fatigue life evaluation of a 5 MW OWT's support structure, and a traditional method and a newly developed optimization technique are both presented to obtain TMD parameters. This optimization technique aims at finding optimal parameters of the TMD which maximizes the fatigue life of a hotspot at the mudline, and effect of time-varying scour can be considered. This study assumes the TMD operates in the FA direction, and the vibration in the SS direction is uncontrolled. Results show that scour can decrease the fatigue life by about 24.1%, and the TMD can effectively suppress vibration and increase the fatigue life. When the scour depth reaches 1.3 times the pile diameter, the TMD with a mass ratio of 1% can increase the fatigue life of OWT's support structure by about 64.6%. Further, it is found that the fatigue life can be extended by 25% with the TMD optimized by the proposed optimization technique, compared to that with the traditionally optimized TMD which does not take the change of dynamic characteristics into account.

Keywords: scour, offshore wind turbine, structural control, modal analysis, fatigue life.

1 Introduction

With the continuous development of large-size fixed-bottom OWTs, local scour and scour protection of pile foundation have become a common issue (L. Wang et al., 2020; X. Wang et al., 2019; F. Zhang et al., 2022). Scour have a significant impact on dynamic characteristics, vibration magnitudes, and thus fatigue life of OWTs under wind and wave loads. On the one hand, the action of currents and waves causes local scour pits around pile foundations, which reduces the burial depth of pile foundations. This phenomenon usually causes a reduction in natural frequencies of OWTs and changes in other dynamic characteristics, possibly leading to resonance, large amplitude stress cycles and fatigue damage when one of natural frequencies is close to the rotational frequency of the blades (Sørensen and Ibsen, 2013). On the other hand,

2

48 current scour protection measures cannot completely avoid scour and have their own

49 shortcomings. For example, armouring protection has the disadvantages that the pro-

50 jectile cannot be accurately cast in complex sea conditions and is easy to be washed

51 away (G. Wang et al., 2023; F. Zhang et al., 2023). Flow-altering protection has the

52 disadvantages of high cost and changing the dynamic characteristics of the foundation

53 (Tang et al., 2023). As offshore structures, wind turbines are vulnerable to corrosion

54 from seawater, which makes the fatigue problem worse (Amirafshari et al., 2021). Thus,

55 the scour-induced changes in dynamic characteristics and risk in resonance inevitably

56 induce a further increase in fatigue damage and deserve in-depth research (Mayall et

57 al., 2018).

58 Many researchers have studied the effect of scour on fatigue damage accumulation

59 in OWTs. For instance, Tempel et al. (2006) investigated the frequency and fatigue of

60 piles under different scour depths and concluded that scour has a little effect on the

61 natural frequencies but a great effect on fatigue damage. Zhang et al. (2021) found that

62 scour depth has a significant influence on monopile impedance. Rezaei et al. (2018)

63 showed that scour leads to an increase in the maximum bending moment of the mono-

64 pile and a shortening of the fatigue life. To mitigate the fatigue damage in OWTs, in-

65 stalling structural control devices is an effective way. It was demonstrated that TMDs

66 have a positive effect on reducing vibration amplitudes of wind turbine systems (Lack-

67 ner and Rotea, 2011a; Dinh and Basu, 2015; Lu et al., 2023; Aydin et al., 2023). Dai et

68 al. (2021) conducted a shaker experiment using a scaled wind turbine model and

69 showed that the installed TMD can suppress the vibration of the structure more effec-

70 tively considering soil-structure interaction (SSI).

71 In the previously mentioned studies, researchers have individually investigated the

72 effect of scour on structural vibration and fatigue, and the structural control by TMDs

73 for OWTs. However, in practice, the effect of scour combining structural control via

74 TMDs could have a significant impact on OWTs' fatigue life. Moreover, whether con-

75 sidering scour could influence the design of TMDs, and TMDs with different parame-

76 ters can also have an impact on fatigue damage accumulation.

77 The purpose of this study is to explore the effect of scour on the fatigue life of

78 wind turbine structures and the control effect of TMD on the fatigue life of wind turbine

79 structures under scour conditions. The authors use a 5 MW single-pile wind turbine as

80 a case study to carry out related research. In this study, ABAQUS is used to establish a

detailed SSI model with different scour depths. A finite element model considering wind loads and TMD was established in MATLAB, and the scour effect is considered by establishing a relationship with the ABAQUS model by means of the equivalent stiffness matrix. And the finite element model is simplified to a modal model for fast prediction of fatigue life. The TMD operates in the FA direction and does not work in the SS direction. This study investigates the effect of different scour depths on the performance of the TMD and the fatigue life of a 5 MW OWT's support structure including a tower and a monopile foundation, and the optimization of the TMD's parameters considering time-varying scour depths to maximum fatigue life is also presented. This study provides some knowledge of the effects of the time varying scour and the TMD on the fatigue life of wind turbines, as well as a new TMD design method targeting at enhancing fatigue resistance. The rest of the paper is organized as follows: Section 2 introduces the numerical models used in the research. Section 3 introduces the traditional TMD design method and the newly developed parameter optimization method. Section 4 describes the load cases for the fatigue analysis, the analysis results of this study and the TMD parameter optimization results. Section 5 concludes the study.

2 Model description

2.1 Finite element model and implementation of tuned mass damper

An FE model of a monopile-supported OWT installed with a TMD is established in MATLAB. This model contains a flexible tower, a rotor-nacelle assembly (RNA), and an external TMD, considering the foundation flexibility. The model is based on the widely used NREL 5MW reference OWT, and its detailed properties are shown in Table 1. Three-dimensional beam elements are used to create the FE model and the theoretical basis is the standard Euler-Bernoulli beam theory. The wind turbine tower is divided into 18 beam elements, and the monopile between the mudline and the mean sea level (MSL) are divided into 4 beam elements. A convergence test by comparing the first natural frequencies shows that 22 beam elements are sufficient. Each element node has 6 degrees of freedom (DOFs) corresponding to the translational and rotational motions in different directions. The mass matrix and stiffness matrix in the equation of motion of the OWT structure can be obtained given the material properties. The damping matrix is applied by means of Rayleigh damping, and the combined damping ratio of soil damping and structural damping is assumed to be 1% (Chen and Duffour, 2018). The Rayleigh mass and stiffness coefficients α_1 and α_2 are defined by $\alpha_1 = \alpha_2 =$

114     $\frac{\zeta_C}{\frac{1}{2\omega}+\frac{\omega}{2}}$. ω is the natural frequency of the first fore-aft mode, and ζ_C is the combined

115   damping ratio. The RNA is represented by a lumped mass at the tower top.
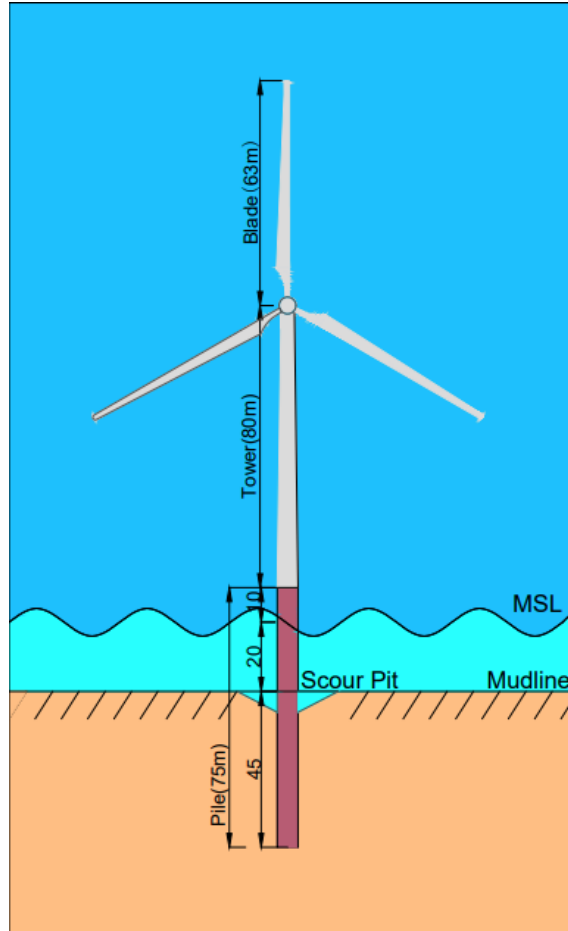
116

117   Fig. 1. Schematic of NREL 5MW wind turbine and scour effect

118   The TMD is mounted on the top of the tower, and the effect of the TMD is consid-

119   ered by adding its mass, damping, and stiffness terms at relevant positions in the local

120   mass, damping, and stiffness matrices of the beam element representing the tower top.

121   The equation of motion of the OWT main structure is:

$$\mathbf{M}_s\ddot{\mathbf{U}}_s + \mathbf{C}_s\dot{\mathbf{U}}_s + \mathbf{K}_s\mathbf{U}_s + \mathbf{C}_T(\dot{\mathbf{U}}_s - \dot{\mathbf{U}}_T) + \mathbf{K}_T(\mathbf{U}_s - \mathbf{U}_T)$$
$$= \mathbf{F}_{\text{wind}} + \mathbf{F}_{\text{wave}}, \tag{1}$$

122   where $\mathbf{M}_s, \mathbf{C}_s, \mathbf{K}_s$ are the mass, damping and stiffness matrices of the main structure.

123     $\mathbf{C}_T, \mathbf{K}_T$ are matrices with same dimensions containing c_T, k_T, $\mathbf{C}_T = \begin{bmatrix} 0 & \cdots & 0 \\ \vdots & \ddots & \vdots \\ 0 & \cdots & c_T \end{bmatrix}, \mathbf{K}_T =$

5

124 $\begin{bmatrix} 0 & \cdots & 0 \\ \vdots & \ddots & \vdots \\ 0 & \cdots & k_T \end{bmatrix}$. $\mathbf{U}_s$ is the displacement vector of the main structure, $\mathbf{U}_s = \begin{bmatrix} u_{s-1} \\ \vdots \\ u_{s-top} \end{bmatrix}$.

125 $\mathbf{U}_T$ is the displacement vector containing u_T, $\mathbf{U}_T = \begin{bmatrix} 0 \\ \vdots \\ u_T \end{bmatrix}$. $\mathbf{F}_{wind}$, $\mathbf{F}_{wave}$ are the aerody-

126 namic and wave load vectors. The equation of motion for the TMD can be represented

127 by

$$m_T \ddot{u}_T + c_T(\dot{u}_T - \dot{u}_{s-top}) + k_T(u_T - u_{s-top}) = 0, \tag{2}$$

128 where m_T, c_T, k_T are the mass, damping and stiffness of the TMD, u_T, u_{s-top} are the

129 displacement of the TMD and the displacement of the top node. The modelling of SSI

130 is realized by an equivalent stiffness matrix, which will be introduced in detail subse-

131 quently in Section 2.3.

132   Table 1. Basic properties of the NREL 5MW reference OWT (J. Jonkman et al.,

133 2009; Rezaei, 2017)

Number of blade	3
Rotor diameter	126 m
Tower length	80 m
Tower diameter	3.87–6.00 m
Tower thickness	28–38 mm
Pile length	75 m
Pile penetration depth	45 m
Pile diameter	6 m
Pile thickness	80 mm
Hub height from MSL	92.4 m
Turbine mass	350000 kg
Blade mass	17740 kg
Rated wind speed	12.1 m/s

134   Wind loads were calculated using modified unsteady blade element momentum

135 (BEM) theory (Branlard, 2017; B. J. Jonkman and Buhl, 2006) with Prandtl and Glauert

136 corrections. Ignoring the iterative loop (Chen, Duffour, Fromme, et al., 2021) in the

137 steady-state BEM code, the instantaneous aerodynamic forces were calculated for each

138 time step within the time integration. The turbulent wind field was generated using the

139 Kaimal spectrum according to the wind field parameters of IEC 61400-3 (2019) as-

140 suming moderate turbulence intensity. It should be noted that the aerodynamic loads

141 from the rotor applied at the tower top were calculated using an aerodynamic force
142 linearization technique previously developed by authors (Chen, Duffour, Fromme, et
143 al., 2021; Chen et al., 2020). This technique divides the aerodynamic loads into two
144 parts. The first part is the quasi-steady aerodynamic force calculated by BEM theory,
145 which does not consider the influence of tower top motion. The second part considers
146 the effect of aerodynamic damping by introducing an additional aerodynamic damping
147 matrix. The adoption of this technique is to enable the development of the simplified
148 modal model for rapid fatigue calculation, which will be introduced in detail in Sub-
149 section 2.4. To represent the influence of controller in the OWT, a standard relationship
150 (J. Jonkman et al., 2009) between the mean wind speed, rotor rotation speed and blade
151 pitch angles, which represents the OWT's normal operational conditions, are adopted
152 throughout the wind loading calculation.
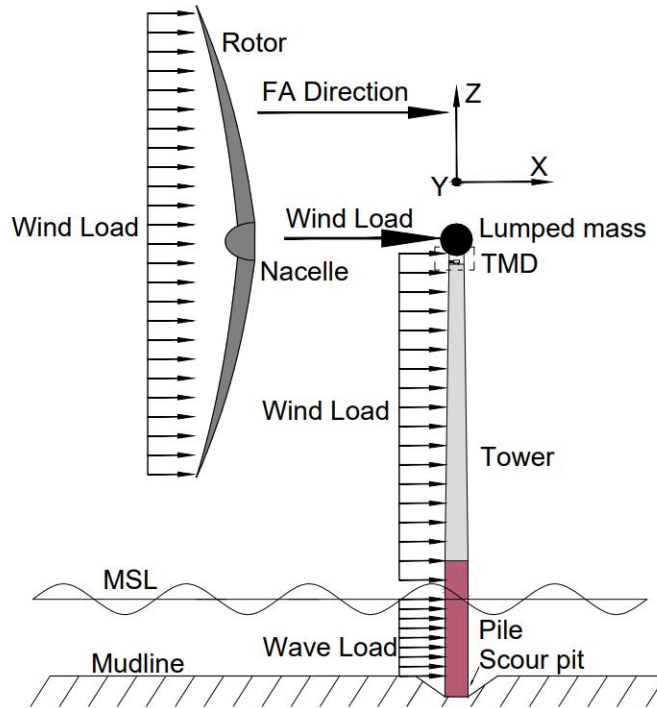
153

154 Fig. 2 Schematic of wind turbine load application

155 Wave loads were calculated using the Morison equation, which includes viscous
156 drag and inertial forces:

$$\mathbf{F}_{\text{wave}} = \frac{1}{2}\rho_w D_{\text{pile}} C_d |\dot{\mathbf{u}}_w| \dot{\mathbf{u}}_w + \frac{\pi}{4}\rho_w D_{\text{pile}}^2 C_m \ddot{\mathbf{u}}_w, \tag{3}$$

157 where $\dot{\mathbf{u}}_w$ and $\ddot{\mathbf{u}}_w$ are the velocity and acceleration of water particles, C_d is the drag

158 coefficient, D_{pile} is the diameter of the monopile between the mean sea level and the

159 mudline, C_m is the inertia coefficient and ρ_w is the density of water. C_d and C_m were

160 chosen as 1 and 2 respectively as the recommended values in Shirzadeh et al (2013).

161 The wave profiles were obtained through the superposition of wave components, com-

162 bining linear wave theory and JONSWAP spectra (Klaus et al., 1973). The application

163 of wind and wave loads is shown in Fig. 2.

## 2.2 Scour modelling in ABAQUS

165   Using solid elements to model pile-soil interaction (S. Dai et al., 2021; Fard et al.,

166 2022; Ma and Chen, 2021; Zdravković et al., 2015) is usually considered to be more

167 accurate than the p-y curve method (Liang et al., 2018; Song and Achmus, 2023) and

168 the equivalent embedding method (Shahmohammadi and Shabakhty, 2020; Bergua et

169 al., 2022). The solid element method can also reduce the influence of empirical formula

170 on the results. Therefore, the solid element method is used to establish the wind turbine

171 scour model. The wind turbine scour model established in ABAQUS contains soil, pile

172 foundation, tower, and the RNA is replaced by a concentrated mass located at the top

173 of the tower. The diameter of the soil body is selected as 20 times of the pile diameter,

174 the soil under the pile foundation is selected as 2.5 times of the pile diameter, and the

175 total height of the soil body is 60 m. The soil body is made of homogeneous dense

176 sandy soil, and the piles and tower are made of steel. The material parameters of the

177 soil body, pile and tower are shown in Table 2 below:

178   Table 2. Soil, pile and tower material parameters

Type	Weight γ （kN/m³）	modulus of elasticity E_S（MPa）	Poisson's ratio υ	Internal friction angle φ（°）	Expansion angle ψ（°）	Cohesion c（kPa）
Soil	19	80	0.3	35	23	0.1
Pile	78.5	215	0.25	-	-	-
Tower	85	215	0.25	-	-	-

179   The Mohr-Coulomb model is used for the soil, and the pile, tower, and nacelle are

180 assumed to be elastic as they are much stiffer than the soil and do not deform plastically

181 for the normal operational conditions. The pile and tower are connected by a binding

182 relationship. The normal contact between the pile and soil adopts the hard contact, and

183 the tangential contact adopts the friction penalty function. The relative sliding friction

184   factor at the interface, μ is equal to $\tan(0.75\varphi)$, where φ is the internal friction angle.

185   The pile-soil contact is in the form of frictional contact, where mutual contact pairs are

186   established between the pile and the soil, including the contacts between the pile bottom

187   surface and the soil, between the outside surface of the pile and the soil, and the inside

188   surface of the pile and the soil core. The frictional contact between pile bottom surface

189   and soil is omitted due to the small area of the contact surface. These frictional contacts

190   all adopt the face-to-face contact, and the contact discretization method adopts the face-

191   to-face discretization method, considering the large stiffness of the main surface and

192   small stiffness of the slave surface. The perimeter of the soil body is translationally

193   constrained, and the bottom surface of the soil adopts a fixed constraint. The eight-node

194   linear brick element (C3D8R) is used to model the pile and soil, and the mesh division

195   is realized by arranging seeds as shown in Fig. 2. The whole model is set up by adopting

196   the modelling method of "element birth and death", which realizes the operation of

197   initial soil stress balance and sets up contacts and other related steps by killing and

198   activating relevant elements.
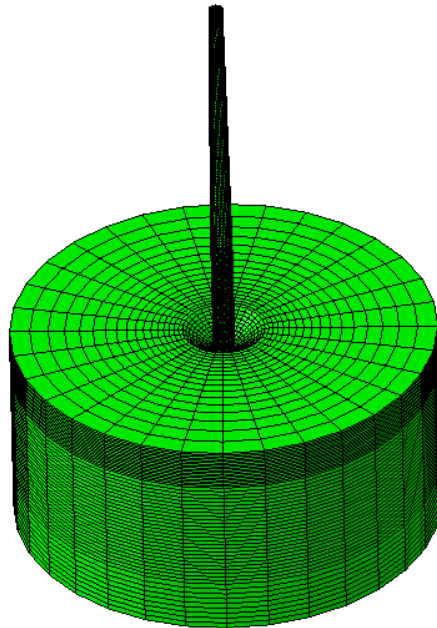
199

200   Fig. 3. Pile-soil interaction modelled by ABAQUS

201   The scour conditions can be represented by a deep conical pit around the pile under

202   the long-term action of the waves and currents. According to the specification of Det

203   Norske Veritas (DNV) (2014b), the radius of the pit surface formed by scour, R, can

204   be related to the depth of the scour pit by

$$R = \frac{D}{2} + \frac{S}{\tan\varphi},$$ (4)

where D is the diameter of the pile, S is the scour depth, and φ is the angle of internal
friction of the soil.

2.3 Equivalent stiffness matrix method

It is necessary to consider the effect of scour in the FE model in MATLAB. An
equivalent stiffness matrix method is adopted in the FE model to consider the flexibility
induced by SSI. The 6 DOFs of node at the mudline are assumed to be constrained by
a series of coupled springs, and the stiffnesses of the coupled springs form a 6×6 stiff-
ness matrix. For one specific stiffness term used in the FE model, for instance the one
relevant to the lateral displacement in the fore-aft (FA) direction, the value of the stiff-
ness term can be found from the relationship between the reaction force at the mudline
and the pile top displacement (Jung et al., 2015). The equivalent stiffness schematic of
the pile-soil interaction in the FA direction for the OWT is shown in Fig. 4.
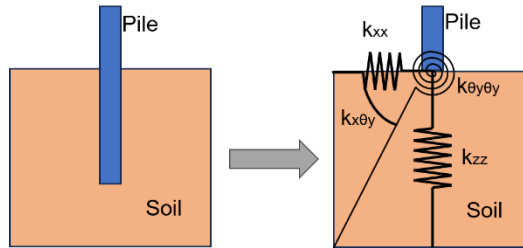
Fig. 4. Equivalent stiffness schematic of pile-soil interaction in the FA direction

According to the principle of virtual displacement and with the DOFs in the other
directions constrained, a unit displacement or rotation was first applied in one direction,
and then the reaction force in that direction can be known. The equivalent stiffness in
that direction can be subsequently calculated by the relationship between the displace-
ment and reaction force. Using the same approach, the stiffness terms corresponding to
the remaining five DOFs were calculated. The stiffness terms in all the six DOFs to-
gether form all the diagonal terms of the soil stiffness matrix. With the diagonal terms
known, the off-diagonal stiffness terms can be found by applying a unit displacement
in one direction and looking at the reaction force in the other concerned direction, with
the other four DOFs constrained. Using the same principle, the off-diagonal terms can
also be found from the relationship between the displacements and reaction forces,

10

which ultimately results in a 6×6 stiffness matrix (Bergua et al., 2021; Pedersen and Askheim, 2021):

$$\mathbf{F_{soil}} = \begin{Bmatrix} F_x(t) \\ F_y(t) \\ F_z(t) \\ M_x(t) \\ M_y(t) \\ M_z(t) \end{Bmatrix} = \begin{bmatrix} k_{xx} & 0 & 0 & 0 & k_{x\theta y} & 0 \\ 0 & k_{yy} & 0 & k_{y\theta x} & 0 & 0 \\ 0 & 0 & k_{zz} & 0 & 0 & 0 \\ 0 & k_{\theta xy} & 0 & k_{\theta x\theta x} & 0 & 0 \\ k_{\theta yx} & 0 & 0 & 0 & k_{\theta y\theta y} & 0 \\ 0 & 0 & 0 & 0 & 0 & k_{\theta z\theta z} \end{bmatrix} \begin{Bmatrix} u_x(t) \\ u_y(t) \\ u_z(t) \\ \theta_x(t) \\ \theta_y(t) \\ \theta_z(t) \end{Bmatrix} \tag{5}$$

$$= \mathbf{K_{soil}u_{soil}} \text{ ,}$$

where $\mathbf{K_{soil}}$ is the equivalent soil stiffness matrix, $\mathbf{u_{soil}}$ is the displacement vector, and $\mathbf{F_{soil}}$ is the reaction force vector. The equivalent soil stiffness matrix ignores the nonlinearity in the force-displacement relationship. This approach is suitable for fatigue analysis, as in normal operation conditions the deformation of the soil around the monopile is relatively small and the nonlinearity in soil stiffness is very weak. The 6×6 soil stiffness matrix obtained from ABAQUS is imported to the FE model in MATLAB. This modelling method possesses the advantages of the increase in accuracy brought by the scour model in ABAQUS with solid elements, and the fast calculation speed and convenience in applying wind and wave loads brought by the usage of the FE model in MATLAB.

2.4 **Rapid fatigue evaluation method**

The established FE model in MATLAB can generate dynamic responses of the OWT, considering wind and wave loads and scour effect. However, a comprehensive fatigue life prediction in time domain needs to consider a large number of environmental states and load cases, so simulation efficiency is very important. Moreover, the TMD design optimization requires much more dynamic response time series. The FE model is not fast enough in this case. Therefore, a simplified modal model is developed from the FE model in MATLAB following the method develop in Ref. (C .Chen et al., 2021). The total aerodynamic forces from the rotor applied on the tower top node are linearized to the sum of a term corresponding to the forces for an assumed rigid tower, plus a term proportional to the tower top linear and angular velocities. The hydrodynamic forces are linearized by ignoring the relatively small monopile vibrations. The details for force linearization can be found in the authors' previous studies (Chen, Duffour, Fromme, et al., 2021). Since the dynamic responses of the OWT are mainly dominated by the first

two bending vibration modes, the FE model is reduced into a 4-DOF simplified modal model by considering only the first two bending modes in the FA and side-side (SS) directions respectively. The development of the simplified 4-DOF modal model is briefly introduced as follows. Denoting the mass matrix and stiffness matrix of the OWT as $\mathbf{M}$ and $\mathbf{K}$ including the TMD and the lumped soil stiffness matrix, the un-damped vibration mode matrix $\mathbf{\Psi}$ can be obtained directly through eigen analysis. According to relationship $\mathbf{u} = \mathbf{\Psi}\boldsymbol{\alpha}$ and multiplying the transpose of the undamped vibra-tion matrix $\mathbf{\Psi^T}$ with the equation of motion, the following equation is obtained:

$$\mathbf{\Psi^T M \Psi \ddot{\alpha} + \Psi^T C \Psi \dot{\alpha} + \Psi^T K \Psi \alpha = \Psi^T F}. \tag{6}$$

Then rewrite the above equation as

$$\mathbf{\bar{M}\ddot{\alpha} + \bar{C}\dot{\alpha} + \bar{K}\alpha = \bar{F}}, \tag{7}$$

where $\boldsymbol{\alpha}$ is the general coordinate vector, $\mathbf{\bar{M}}$ is the modal mass matrix, $\mathbf{\bar{C}}$ is the modal damping matrix, $\mathbf{\bar{K}}$ is the modal stiffness matrix, $\mathbf{\bar{F}}$ the modal load matrix. Truncating Eq. (6) by only considering the first two bending modes, the FE model is reduced to a 4-DOF modal model, which can be used for a rapid fatigue analysis. The dynamic re-sponses of the OWT can be obtained by modal superposition after solving the general coordinate vector by time integration. In the 4-DOF simplified modal model, the cross-section stress at any height can be calculated from the calculated node displacements. According to the dynamic stress extraction method provided by Pelayo et al. (Pelayo et al., 2015), the cross-section stress $\sigma_Z(t)$ at any moment at a given location can be ob-tained by:

$$\sigma_Z(t) = -E\big(\mathbf{N}^{e''}(z)\mathbf{u}_x^e(t)x + \mathbf{N}^{e''}(z)\mathbf{u}_y^e(t)y\big), \tag{8}$$

where $\mathbf{u}^e$ is the nodal displacement vector at the cross section, E is the material elastic modulus, and $\mathbf{N}^e$ is the elemental shape function vector of FE model, x and y are the positions within the section at the height z of the tower. After cyclic counting the stress time series using the rainfall counting method, the fatigue damage at the hotspot can be evaluated by utilizing the Palmgren-Miner rule based on the S-N fatigue calculation method. The S-N curve for steel under water can be obtained by the following equation considering the thickness effect in DNV (2014a):

$$logN = log\bar{a} - m \cdot log\left[\Delta\sigma\left(\frac{t}{t_{ref}}\right)^k\right],\qquad(9)$$

282   where N is the number of cycles to failure, $\Delta\sigma$ is the stress range. $\Delta\sigma$ is calculated from

283   the nominal stress $\Delta\sigma_{nominal}$ by the equation $\Delta\sigma = SCF \cdot \Delta\sigma_{nominal}$, SCF is the stress

284   concentration factor. m is the negative inverse slope of the S-N curve, and $log\bar{a}$ is the

285   intercept between the log N axis and the S-N curve, t_{ref} is the reference thickness for

286   welded joints, t is the thickness at which cracks may grow. And $t = t_{ref}$ is used for

287   thickness less than t_{ref}. When t is larger than t_{ref}, t is the actual thickness of the pile. k

288   is the thickness exponent of fatigue strength. For pile joints, $t_{ref} = 25mm$. According

289   to the DNV code, a bilinear S-N curve is usually used for offshore structures subjected

290   mainly to typical wind and wave loads, using the Class E structural detail S-N curve

291   shown in Table 3.

292   Table 3 Class E structural detail S-N curves

$N \leq 10^6$		$N \geq 10^6$				
m_1	$log\bar{a}_1$	m_2	$log\bar{a}_2$	k	t（mm）	SCF
3.0	11.610	5.0	15.350	0.2	80	1.13

293   For variable amplitude stresses, the fatigue damage index is calculated using the

294   Palmgren-Miner summation rule:

$$D_k = \sum_{i=1}^{N_c} \frac{n_i}{N_i},\qquad(10)$$

295   where N_c is the total number of bins, n_i is the number of cycles in i^{th} stress bin, N_i is

296   the number of cycles to failure for the ith stress range, and D_k is the total fatigue dam-

297   age index. The "rainflow" function in MATLAB is adopted for rainflow counting.

298   When a stress time history is given, this function can automatically obtain the ith stress

299   range and the corresponding cycle number n_i, and N_c is the total number of stress

300   ranges. Fatigue failure occurs at the hotspot when the fatigue damage index reaches

301   unit 1.

302   3 **Damper design and optimisation method**

303   Installing damping devices can efficiently reduce the vibration amplitudes of

304   OWTs so that their service life can be greatly prolonged. Using TMDs as passive

305 control devices is most widely used to control the vibration of OWT support structures.

306 Usually, most of TMDs are designed according to the dynamic characteristics of the

307 OWTs determined in the preliminary design stage, without considering the changes in

308 dynamic properties possibly caused by scour and soil degradation. However, in the real

309 environment, scour can cause the dynamic characteristics of OWTs to change, which

310 perhaps makes installed dampers become less effective or even completely ineffective.

311 Therefore, it is a great significance to consider the change in dynamic properties caused

312 by scour on the TMD design. The following two subsections first introduce the tradi-

313 tional TMD design method considering constant dynamic characteristic in the initial

314 state, and then an optimal parameter searching method for the design of TMDs is pre-

315 sented considering the effect of scour and fatigue life evaluation.

316 ## 3.1 TMD design in initial state
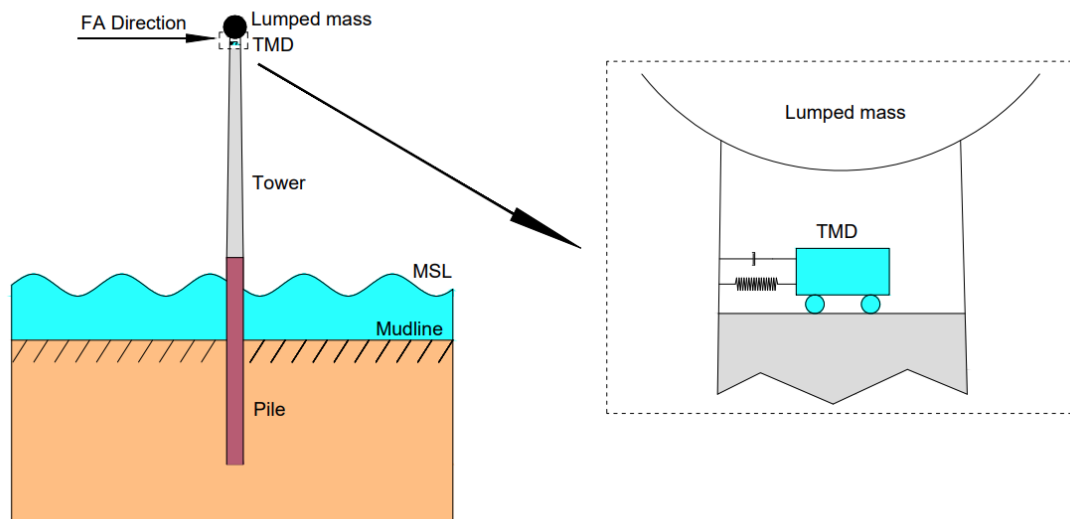
317

318 Fig. 5. Schematic diagram of TMD arrangement in the tower tube

319 As the dominant vibration mode of the OWT structure in operation is the first

320 bending mode, the largest vibration amplitude occurs at the tower top and installing the

321 TMD at the tower top is most effective. Therefore, the TMD is installed inside the steel

322 tube at the tower top to mainly control the vibration in the FA direction, as shown in

323 Fig. 5. And the TMD can be aligned with the FA direction by rotating the damper.

324 Accordingly, the initial design of the TMD is mainly carried out based on the dynamic

325 properties for the first-order mode. The initial design is conduct based on the assump-

326 tion that the monopile foundation is not scoured.

14

327   Numerous studies have shown that a TMD can effectively suppress the vibration
328   of a main structure when the mass ratio of the TMDs to the main structure is 1%-2%
329   (Lackner and Rotea, 2011b; R. Zhang et al., 2019). After determining the mass ratio of
330   the TMD to the OWT structure, according to the classic TMD optimization theory
331   proposed by Den Hartog (1957), the optimal frequency ratio of the TMD to the OWT
332   structure is

$$\alpha_{opt} = \frac{1}{1 + \mu}. \tag{11}$$

333   The optimal damping ratio for the TMD can be calculated by

$$\xi_{opt} = \sqrt{\frac{3\mu}{8(1 + \mu)}}, \tag{12}$$

334   where μ is the mass ratio of the TMD to the OWT structure, α_{opt} is the optimal fre-
335   quency ratio of the TMD to the OWT structure and α_{opt} is the optimal damping ratio
336   of the TMD.

337   Considering that excessive mass will lead to increased construction costs and dif-
338   ficulties and changes in the inherent characteristics of the original structure, the mass
339   ratio of the TMD system to the main structure is first selected to be 1%. Moreover,
340   previous studies have found that TLCD with a mass ratio of 1% and TMD with a mass
341   ratio of 2% can effectively suppress vibration (Colwell and Basu, 2009; Lackner and
342   Rotea, 2011b; R. Zhang et al., 2019). According to Den Hartog's optimization theory
343   for the initial TMD design, it can be determined that the optimal frequency ratio of the
344   TMD to the main structure is 0.99, and the optimal damping ratio of the TMD is 0.061.
345   When the OWT support structure is not scoured, the first-order modal mass of the struc-
346   ture is 440350 kg, and the first-order modal frequency is 0.265 Hz. Therefore, accord-
347   ing to the initial design parameters, the mass, stiffness coefficient and damping coeffi-
348   cient of the TMD system are 4403.5 kg, 11,952 N/m and 885 Ns/m respectively.

349   3.2 **Fatigue-based damper optimisation technique**

350   After scour occurs around the monopile foundation, the burial depth of the mono-
351   pile and natural frequencies of the OWT gradually change. The vibration mitigation
352   effect of the TMD designed based on the dynamic parameters in the initial state can be

reduced, which may lead to the increase of fatigue damage of the OWT support structure. Therefore, when designing the TMD, considering the influence of the time-varying scour can enhance the performance of the TMD and thus result in a longer fatigue life of the support structure.
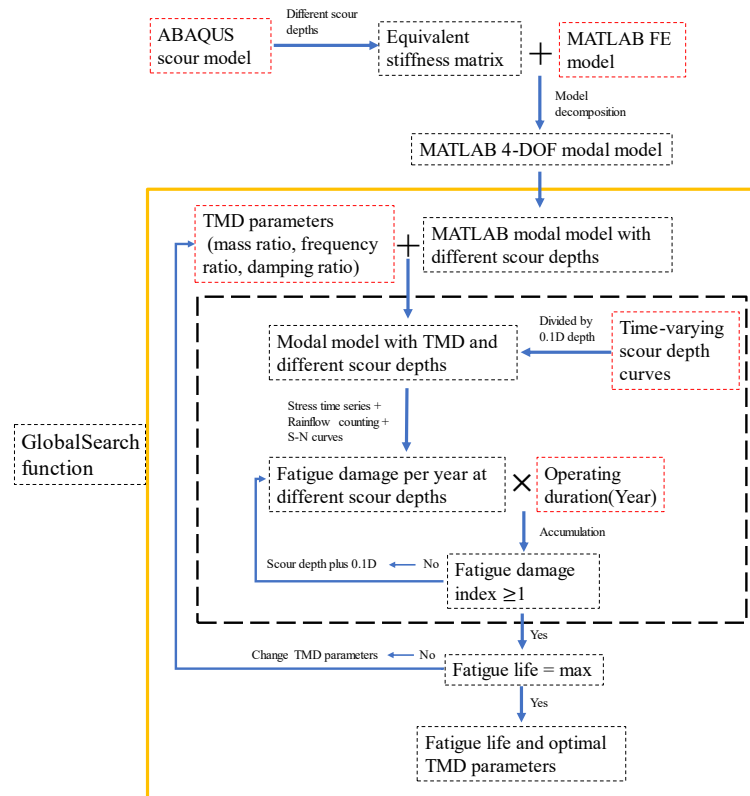
Fig. 6. Flowchart of TMD fatigue-life-based optimization technique

Here a fatigue-life-based optimization technique (FOT) to find optimal parameters of the TMD is developed in MATLAB as shown in Fig. 8. In this technique, the frequency ratio, mass ratio and damping ratio of the TMD are set as the optimal parameters to search, and the fatigue life is the optimization objective. When considering the time-varying scour process, the time-varying scour depth curve is first divided into a number of scour depths with an increment of 0.1d. For each scour depth, the fatigue damage is calculated respectively and then the total fatigue damage in a particular duration can be summarised. When the scour pit becomes deeper, the fatigue damage accumulates and finally reaches unit 1 which denotes the end of fatigue life. The simplified 4-DOF modal model incorporating scour modelling is used to generate the stress time series. The optimization problem is formed so that the optimal parameters of the TMD correspond to the longest fatigue life of the OWT support structure. The GlobalSearch function in MATLAB was used to solve the optimization problem. In the TMD optimization

16

process, the mass ratio of TMD is first set to 1%, and only the parameter frequency ratio and damping ratio are optimized. Subsequently, in order to understand the optimization effect of TMD when the value of TMD mass ratio is not fixed, a mass ratio optimization interval is given, so the mass ratio becomes a variable within the optimization interval.

4 Results

4.1 Environmental states and load cases

In this study, fatigue analyses are performed under 22 environmental states provided by Tempel (2006), taking into account both operational and parked conditions. These 22 environmental states are shown in Table 4. In operating conditions, the wind turbine bears the aerodynamic load of the rotating rotor and the wind load of the tower, and the wind load on the rotor is calculated using the BEM theory. In parked conditions, the wind turbine mainly bears the aerodynamic load on the tower, and the aerodynamic damping is very small. The aerodynamic loading on the blades is calculated by directly looking at the aerodynamic loading coefficient table given the local attack angles. The wind and wave loads are assumed to be always in the same direction to simplify the analysis. When the mean wind speeds are above the cut-in wind speed and below the cut-out wind speed, a 95% wind turbine availability is assumed following the setting in Ref (Velarde et al., 2020), meaning that the OWT does not produce power for 5% when the mean wind speeds are in the operating range. For a particular set of mean wind speed, wave period and wave height, six different random seed numbers are used to generate different wind fields and wave profiles to reduce the influence of randomness. To obtain the stress time histories at the mudline, a 700s simulation for each random seed was conducted and the response in the first 100 seconds was deducted to eliminate the effect of initial transient vibration. (Capaldo and Mella, 2023; Stieng and Muskulus, 2020).

Table 4. Environmental states, adopted from Tempel (van der Tempel, 2006).

State	Vw (m/s)	Tz (s)	Hs (m)	P_{State} (%)	State	Vw (m/s)	Tz (s)	Hs (m)	P_{State} (%)
1	4	3	0.5	3.95	12	14	5	2	3.26
2	4	4	0.5	3.21	13	16	4	2	1.79
3	6	3	0.5	11.17	14	16	5	2.5	3.1
4	6	4	0.5	7.22	15	18	5	2.5	1.74

5	8	3	0.5	11.45	16	18	5	3	0.8
6	8	4	1	8.68	17	20	5	2.5	0.43
7	10	3	0.5	5.31	18	20	5	3	1.14
8	10	4	1	11.33	19	22	5	3	0.4
9	12	4	1	5.86	20	22	6	4	0.29
10	12	4	1.5	6	21	24	5	3.5	0.15
11	14	4	1.5	4.48	22	24	6	4	0.1

399   In Table 4, V_w is the wind speed, T_z is the zero-crossing wave period, H_s is the

400   wave height, and P_{state} is the probability of environmental state. To investigate the ef-

401   fect of scour and installation of the TMD on the fatigue damage accumulation, six load

402   cases (LCs) are selected as shown in Table 5. LC 1 is used as the reference case, and

403   other cases are distinguished by different scour and TMD settings. For LC 4 to LC 6,

404   the initial design of the TMD with the mass ratio of 1% is used.

405   Table 5. Load case definition

LC number	TMD condition	Scour condition	LC number	TMD condition	Scour condition
LC 1	No	No Scour	LC 4	Enable	No Scour
LC 2	No	Time-varying	LC 5	Enable	Time-varying
LC 3	No	Maximum	LC 6	Enable	Maximum

406   When considering the time-varying scour depth, for a particular time t, the time-

407   varying scour depth S can be predicted by the equation provided by Nakagawa et al.

408   (1976):

$$S = \left(\frac{t}{t_1}\right)^{0.22} D, \tag{13}$$

409   where D is the diameter of the monopile, t_1 is the reference time and can be calculated

410   by

$$t_1 = 29.2 \cdot \frac{D}{\sqrt{2} \cdot u} \cdot \left(\frac{\sqrt{\Delta \cdot g \cdot d_{50}}}{\sqrt{2} \cdot u - u_c}\right)^3 \cdot \left(\frac{D}{d_{50}}\right)^{1.9}. \tag{14}$$

411   u is the tidal velocity and taken as 0.5 m/s, u_c is the critical shear velocity and taken as

412   0.37 m/s, g is the acceleration of gravity and taken as 9.8 m/s^2, d_{50} is grain size of sea

413   sand and taken as 0.2 mm. The parameter $\Delta = \frac{\rho_s}{\rho_w} - 1$, where ρ_s is density of sand and

414   taken as 2.65 g/cm^3, ρ_w is density of water and taken as 1 g/cm^3. Rudolph et al.

415 (Rudolph et al., 2016) provided the sea state and measured the scour depth for the North
416 Sea where the monopile N7 is located. The measured scour depth was fitted well for
417 the first five years based on the time-varying scour depth prediction equation shown in
418 Eq. (13). Therefore, the data from the North Sea site can represent a typical ocean en-
419 vironment with time-varying scour and is used for the correlation analysis in this study.
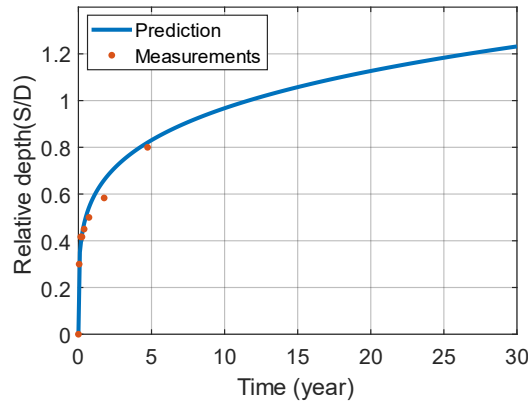
420

421 Fig. 7. Time-varying scour depth curve for pile N7 in the North Sea

422 When conducting analysis with the time-varying scour, an increment of scour
423 depth equal to 0.1D is used. At one particular scour depth, the fatigue damage is calcu-
424 lated and then the total fatigue damage during a longer period with a changing scour
425 depth can be obtained by damage accumulation. According to the specification of DNV,
426 the maximum depth of a local scour pit formed around a pile foundation is 1.3 times
427 the diameter of the pile. Therefore, it is assumed that the local scour pit has a maximum
428 scour depth of 1.3D at which the scour process achieves equilibrium.

429 4.2 **Scour influence on natural frequencies**

430 The scour of the soil around the monopile has an important effect on the natural
431 frequencies of the OWT. For different scour depths, the first natural frequencies ob-
432 tained the by the models in ABAQUS and MATLAB are compared in Fig. 8. It shows
433 the increase in the scour depth leads to a decrease in the first natural frequency of the
434 OWT. The first natural frequency is 0.265 Hz when no scour occurs, and the natural
435 frequency is reduced to 0.248 Hz when the depth of the scour pit reaches the maximum
436 depth. The first natural frequency is reduced by 6.42% due to the maximum scour depth.
437 It shows that the natural frequency nearly monotonically decreases with the increase of
438 the scour depth. The installation of TMD also influences the natural frequency of the
439 OWT main structure. The TMD with a mass ratio of 1% makes the first natural

440   frequency of the OWT main structure reduces to 0.251 Hz when no scour occurs, mean-

441   ing that the natural frequency is reduced by 5.28%.
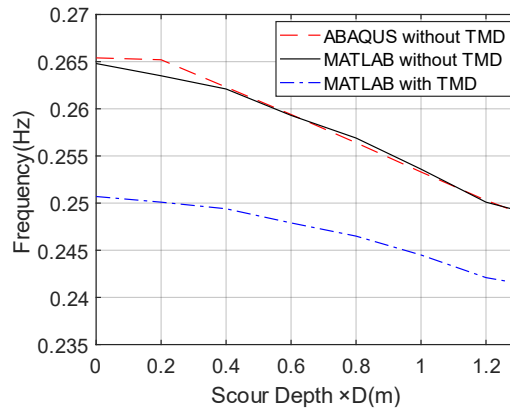
443   Fig. 8. Relationship between wind turbine natural frequency and scour depth

444   In the TMD design process, the feasible displacement should be considered. The

445   smaller the mass ratio of TMD is, the larger the feasible displacement is required. The

446   22nd environmental state corresponds to the greatest vibration responses of the wind

447   turbine tower top due to large wind speed variations and lower aerodynamic damping,

448   and the stroke of the TMD could be the largest. As shown in the Fig. 9, the relative

449   displacement between the TMD and the tower top is much less than the inner diameter

450   of the wind turbine tower top in the 22nd environmental state. It shows that the stroke

451   of the TMD is sufficient when the mass ratio of TMD is 1%.
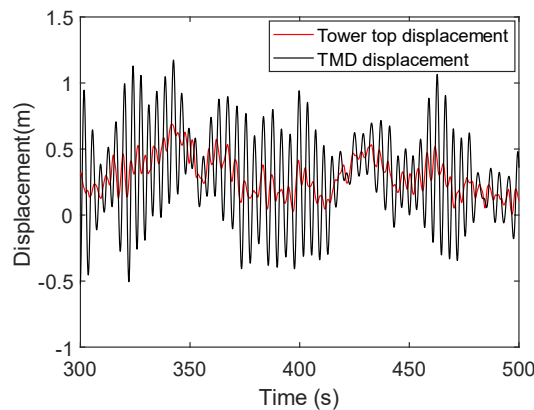

453   Fig. 9 Displacement of tower top and TMD under the 22nd environmental state

454   4.3 **Dynamic response analysis**

455   When the OWT in the operating state is under the 9th environmental state which

456   corresponds to the rated wind speed of 12 m/s, a comparison for the tower top displace-

457   ments is made for LC 1, LC 3, LC 4 and LC 6, as shown in Fig. 10. These displacements

20

are obtained from the FE model in MATLAB described in Subsection 2.1. By comparing the displacements from 300 seconds to 420 seconds for LC 1 and LC 4, it can be found that the displacement amplitudes of the tower top decreases when the TMD is installed. It is known that the aerodynamic damping is large when the OWT is operating under the rated wind speed, so it is normal that the vibration mitigation effect of the TMD is less significant in this case.
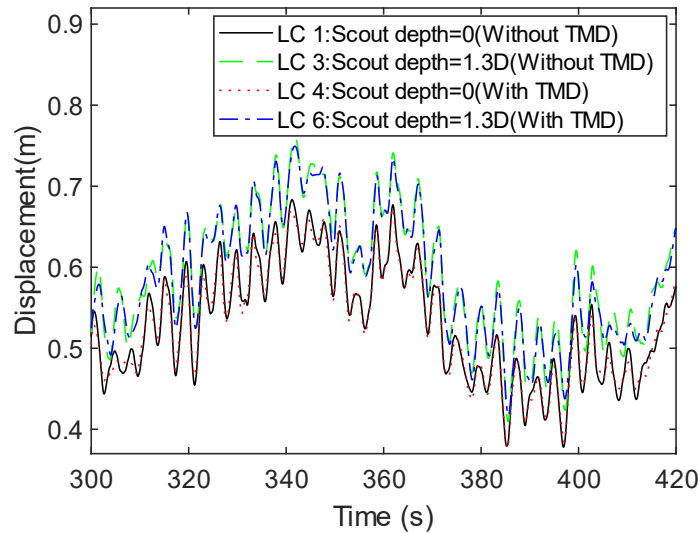
Fig. 10. Dynamic response of wind turbine under wind-wave coupled loads for four operating conditions
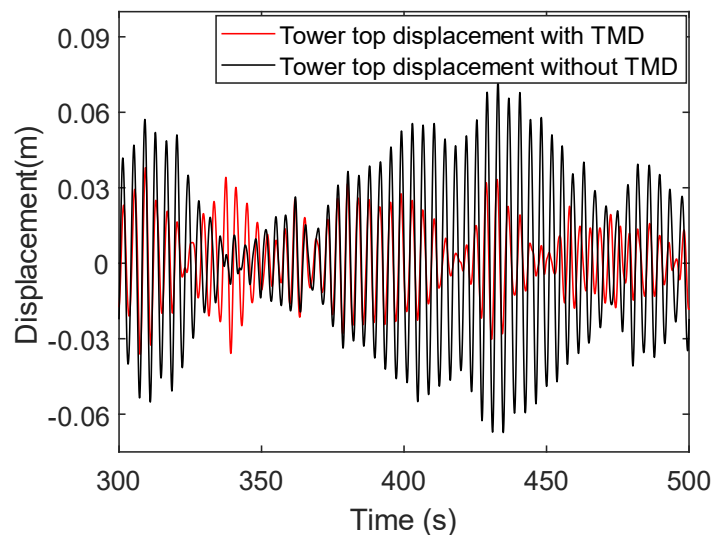
Fig. 11 The displacement response of wind turbine tower under the parked condition with 3 m/s wind speed

21

470 The effect of the TMD is more prominent for parked conditions with less aerody-
471 namic damping. As shown in the Fig. 11, the vibration mitigation effect of the TMD is
472 more significant under the parked condition with 3 m/s wind speed. Moreover, by com-
473 paring the displacement responses for LC 1 and LC 3, it can be found that the average
474 of the displacement at the tower top increases when the scour depth reaches 1.3D. This
475 is because scour makes the OWT support structure become more flexible.

476 ### 4.4 Fatigue calculation results

477 In Subsection 2.4, it is mentioned that in the process of fatigue life analysis, the 4-
478 DOF simplified modal model is used to greatly save the calculation time. The accuracy
479 test of the 4-DOF modal model in generating dynamic responses is first present in this
480 subsection. Under the turbulent wind field with a turbulence intensity of 11.9% and an
481 average wind speed of 12 m/s, the FE model and the 4-DOF simplified modal model
482 are used to calculate the stress responses at the mudline for 10 minutes.

483 As shown in Fig. 12, the stress responses from these two models are very close,
484 confirming good accuracy of the 4-DOF modal model. The fatigue damage caused by
485 the FE model in 10 min is 2.108×10^{-7}, and the fatigue damage caused by the 4-DOF
486 model in 10 min is 2.1×10^{-7}, with an error of 0.05%. Moreover, the calculation time
487 of the 4-DOF simplified modal model is only about 1/55 of that of the FE model, which
488 shows that the 4-DOF simplified modal model is adequate to replace the FE model
489 when conducting fatigue life prediction.

(a)   (b)
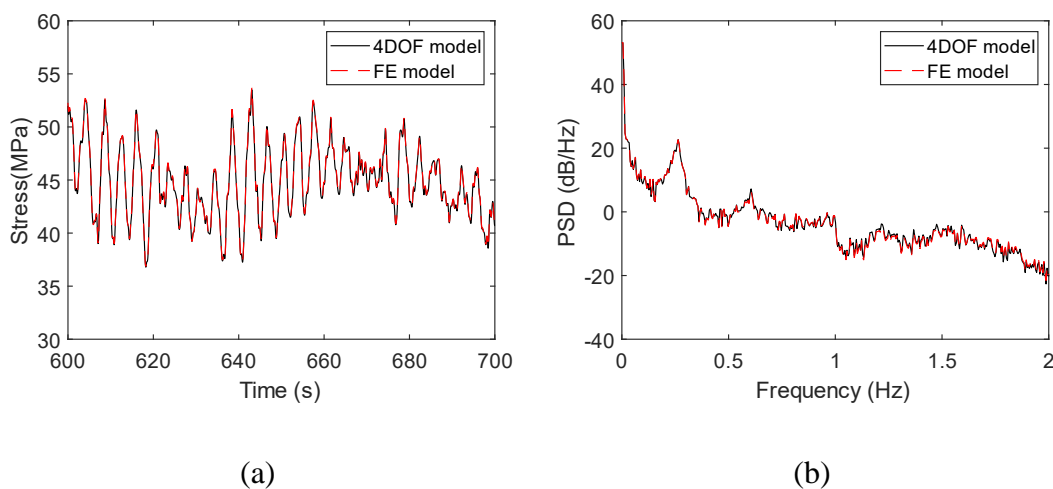
490 Fig. 12. Comparison of stresses at the mudline from the FE model and the 4-DOF
491 model in time domain (a) and frequency domain (b)

492   The 4-DOF simplified modal model is used to conduct fatigue life prediction for

493   the OWT support structure under LC 1 to LC 6. A 10 min simulation for each random

494   seed of is six different random seed numbers conducted to obtain the stress time histo-

495   ries at the mudline. The location of the hotspot used to evaluate fatigue damage is se-

496   lected at the point where the maximum stress is reached, and this point is in the support

497   structure cross section at the mudline. Although the location in the monopile where the

498   moment reaches its maximum value can be below the mudline, the location at the mud-

499   line is picked for simplicity. Further, as the SSI is modelled in the FE model by an

500   equivalent soil stiffness matrix, it is unstraightforward to obtain the internal forces at

501   the cross sections below the mudline. Given the stress time series at the selected hotspot,

502   the corresponding fatigue damage is calculated. Then the fatigue damage for the set of

503   mean wind speed, wave period and wave height in 10 min is obtained by averaging the

504   fatigue damage for all the six random seeds. For all the 22 environment states, the 10

505   min fatigue damage are calculated, and the fatigue life is predicted according to

506   Palmgren-Miner sum rule by combing these calculated fatigue damage and the occur-

507   rence probabilities of the environmental states.

508   For different scour depths, the fatigue life of the OWT considering both operating

509   and parked conditions is predicted with or without TMD installation, and the results are

510   shown in Fig. 13. It is shown that an increase in scour depth leads to a decrease in

511   fatigue life, and an increasing fatigue life reduction rate can be observed when the scour

512   depth increases. When no scour occurs and the TMD is not installed on the OWT, the

513   OWT's fatigue life is 59.3 years, and the fatigue life drops to 45.0 years when consid-

514   ering the maximum scour depth of 1.3 D. There exist some uncertainties in the fatigue

515   life prediction process due to the generation of random wind field and wave profile. It

516   should be noted that the predicted fatigue life is much longer than the normally adopted

517   OWTs' design fatigue life of 25-30 years. This can be explained by the following rea-

518   sons. First, the maximum moment of the OWT support structure is not at the cross

519   section at the mudline where the selected hotspot is located. Second, the complex wind

520   and wave directionality during the OWT's lifetime is simplified, which would influence

521   the fatigue calculation result. Third, many other operation conditions such as starting

522   up, shutting down phases are not considered in this study, which can also have an im-

523   pact on the fatigue damage accumulation. Moreover, the installation of the TMD greatly

524   extends about 51.8% of the OWT support structure's fatigue life.

525
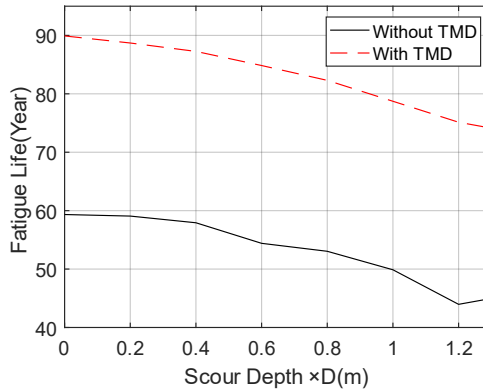
Fig. 13. Fatigue life of wind turbine with different scour depths

526

527 The fatigue life prediction results of the OWT were obtained for all the six LCs,
528 as shown in Fig. 14. The fatigue life from the reference case LC 1, 59.3 years, is re-
529 garded as the reference fatigue life. It shows that the fatigue life decreases by 14.3 years,
530 or about 24.1%, when the scour depth is set as the maximum value of 1.3D without
531 applying the TMD, compared to the reference fatigue life. When considering the time-
532 varying scour, the fatigue life decreases by about 22.1% from the reference value. When
533 comparing the results for LC 1 and LC 4, it shows the installation of the TMD results
534 in a significant increase in the fatigue life of the OWT, with an increase in fatigue life
535 of about 30.7 years, which is about 51.8%. In LCs with the TMD installed, the fatigue
536 life in LC 6 decreases by about 17.7% when the scour depth reaches 1.3 D, compared
537 to the result in LC 4. But the fatigue life in LC 6 is still 1.25 times of the reference
538 fatigue life, which indicates that the imposition of TMD can effectively increase the
539 fatigue life of the OWT by reducing vibration amplitudes.

540
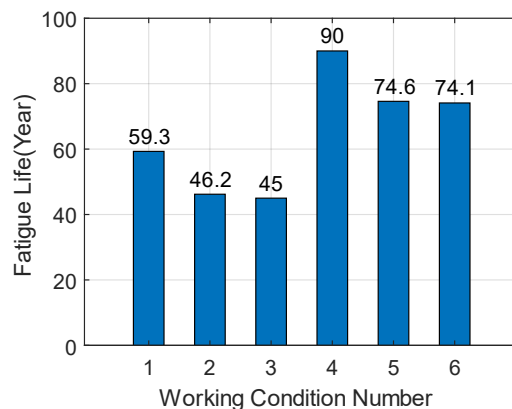
541 Fig. 14. Fatigue life of the wind turbine under six operating conditions

542 ### 4.5 **Fatigue calculation with optimized TMD**

543   To compare the optimization effect and speed up the optimal parameter search

544 process, the mass ratio of TMD is first kept as 1%. Before the optimization, the param-

545 eter ranges of the frequency ratio and damping ratio need to be defined. The optimal

546 frequency of the TMD is usually close to the resonance frequency of the main structure,

547 so the range of the frequency ratio was chosen to be from 0.8 to 1.1 for optimization.

548 As the optimal damping ratio could vary in a relatively larger range, the range of the

549 damping ratio for optimization is chosen to be from 1% to 30%. The optimization of

550 the TMD is also conducted with the mass ratio not fixed. A range of the mass ratio from

551 0.001 to 0.1 is used to optimize the TMD so that the influence of the mass ratio can be

552 evaluated.

553 <div align="center">Table 6. Optimization of TMD parameters</div>

Optimization method	Mass ratio range	Time-varying scour	Optimal mass ratio	Optimal frequency ratio	Optimal damping ratio	Fatigue life （Year）
Initial (LC 5)	0.01	Use	0.01	0.99	0.061	74.6
FOT	0.01	Use	0.01	0.94	0.050	93.2
FOT	0.001-0.1	Use	0.097	0.92	0.150	133.2

554   The optimal parameters obtained by FOT as well as the predicted fatigue life are

555 listed in Table 6. The fatigue life for LC 5 and the parameters of the initially designed

556 TMD are also shown in Table 6 for comparison. It shows that when the mass ratio is

557 fixed at 1%, the optimal frequency ratio is 0.94, the optimal damping ratio is 5%, and

558 the final fatigue life is 93.2 years. Compared to the fatigue life with initially optimized

559 TMD using the traditional method without considering scour, the fatigue life is in-

560 creased by 18.6 years or about 25%. It indicates that the parameter search in the opti-

561 mization process is correct and it is better to use the TMD parameter search method to

562 design the TMD after obtaining the time-varying scour curve. When the mass ratio

563 range is taken from 0.1% to 10%, the optimal mass ratio of the TMD is 9.7%, the fre-

564 quency ratio is 0.92, the damping ratio is 15%, and the final fatigue life is 133.2 years.

565 In this case, the fatigue life of the OWT is significantly increased mainly due to the

566 large mass ratio. However, in practice, it might be uneconomic to implement a TMD

567 with such a large mass ratio.

5 Conclusions

This study establishes a rapid numerical model which can consider the effect of scour and installation of a TMD, and the TMD operates only in the FA direction. The model is simplified by using concentrated mass instead of RNA and ignores the non-linearity of the equivalent stiffness matrix. The established model is used to investigate the influence of scour and the installed passive structural control device on the OWT's natural frequencies and fatigue life through 22 environmental states. An optimization technique is also developed to find optimal parameters of the TMD considering time-varying scour. Moreover, it shows that the vibration amplitude of the OWT can be effectively reduced by the TMD. On the one hand, results show that the TMD reduces the vibration amplitude of the tower top. On the other hand, when the scour depth reaches 1.3D, the wind turbine support structure becomes more flexible, with the displacement of the tower top increased without TMD.

In addition, the fatigue calculation results show that installation of the TMD significantly extends the fatigue life of the OWT, but scour can cause a reduced performance of the TMD. It is found that when the initially designed TMD does consider scour and the scour-induced natural frequency reduction during the OWT's lifetime, its performance is not as good as the TMD optimized by the developed FOT in terms of fatigue life enhancement. Given a mass ratio of 1%, the fatigue life can be extended by 25% with the TMD optimized by FOT. This is because FOT can consider the effect of time-varying scour. This study only performs the analysis with scour, but other factors such as soil degradation can also alter the dynamic characteristics of OWTs and thus have some influence on structural control devices' performance and fatigue life evaluation. Additionally, during OWTs' lifetime, the properties of installed TMDs can also change, making the evaluation of TMDs' performance and OWTs' fatigue life more complicated. These factors are worthwhile investigating in the future.

6 Competing interests

The contact author has declared that none of the authors has any competing interests.

7 Acknowledgements

602

603

604

605

606

607

References

Amirafshari, P., Brennan, F. and Kolios, A. (2021). A fracture mechanics framework for optimising design and inspection of offshore wind turbine support structures against fatigue failure. Wind Energy Sci., 6(3), 677–699. https://doi.org/10.5194/wes-6-677-2021

Aydin, E., Öztürk, B., Kebeli, Y. E. and Gültepe, G. (2023). An Experimental Study on the Effects of Different Pendulum Damper Designs on Structural Behavior. In G. P. Cimellaro (Ed.), Seismic Isolation, Energy Dissipation and Active Vibration Control of Structures (Vol. 309, pp. 240–253). Cham: Springer International Publishing. https://doi.org/10.1007/978-3-031-21187-4_18

Bergua, R., Robertson, A., Jonkman, J. and Platt, A. (2021). Specification Document for OC6 Phase II: Verification of an Advanced Soil-Structure Interaction Model for Offshore Wind Turbines (NREL/TP--5000-79938; p. NREL/TP--5000-79938).

Bergua, R., Robertson, A., Jonkman, J., Platt, A., Page, A., Qvist, J., Amet, E., Cai, Z., Han, H., Beardsell, A., et al. (2022). OC6 Phase II: Integration and verification of a new soil–structure interaction model for offshore wind design. Wind Energy, 25, 793–810.

Branlard, E. (2017). Wind Turbine Aerodynamics and Vorticity-Based Methods: Fundamentals and Recent Applications (Vol. 7). Cham: Springer International Publishing.

Capaldo, M. and Mella, P. (2023). Damping analysis of floating offshore wind turbines (FOWTs): a new control strategy reducing the platform vibrations. Wind Energy Sci., 8(8), 1319–1339. https://doi.org/10.5194/wes-8-1319-2023

Chen, C. and Duffour, P. (2018). Modelling damping sources in monopile-supported offshore wind turbines. Wind Energy, 21(11), 1121–1140. https://doi.org/10.1002/we.2218

Chen, C., Duffour, P., Dai, K., Wang, Y. and Fromme, P. (2021). Identification of aerodynamic damping matrix for operating wind turbines. Mech. Syst. Signal Process., 154, 107568. https://doi.org/10.1016/j.ymssp.2020.107568

Chen, C., Duffour, P. and Fromme, P. (2020). Modelling wind turbine tower-rotor interaction through an aerodynamic damping matrix. J. Sound Vib., 489, 115667. https://doi.org/10.1016/j.jsv.2020.115667

Chen, C., Duffour, P., Fromme, P. and Hua, X. (2021). Numerically efficient fatigue life prediction of offshore wind turbines using aerodynamic decoupling. Renew. Energy, 178, 1421–1434. https://doi.org/10.1016/j.renene.2021.06.115

Colwell, S. and Basu, B. (2009). Tuned liquid column dampers in offshore wind turbines for structural control. Eng. Struct., 31(2), 358–368. https://doi.org/10.1016/j.engstruct.2008.09.001

Dai, K., Huang, H., Lu, Y., Meng, J., Mao, Z. and Camara, A. (2021). Effects of soil–structure interaction on the design of tuned mass damper to control the seismic response of wind turbine towers with gravity base. Wind Energy, 24(4), 323–344. https://doi.org/10.1002/we.2576

651 Dai, S., Han, B., Wang, B., Luo, J. and He, B. (2021). Influence of soil scour on lateral
652   behavior of large-diameter offshore wind-turbine monopile and corresponding
653   scour monitoring method. Ocean Eng., 239, 109809.
654   https://doi.org/10.1016/j.oceaneng.2021.109809

655 Den Hartog, J. P. (1957). Mechanical Vibrations. Fourth Edition. Aeronaut. J., 61(554),
656   139–139.

657 Dinh, V.-N. and Basu, B. (2015). Passive control of floating offshore wind turbine na-
658   celle and spar vibrations by multiple tuned mass dampers. Struct. Control Health
659   Monit., 22(1), 152–176. https://doi.org/10.1002/stc.1666

660 DNVGL-RP-0005. (2014a). RP-C203: Fatigue design of offshore steel structures.

661 DNV-OS-J101. (2014b). Design of Offshore Wind Turbine Structures.

662 Fard, M. M., Erken, A., Erkmen, B. and Ansal, A. (2022). Analysis of Offshore Wind
663   Turbine by considering Soil-Pile-Structure Interaction: Effects of Foundation
664   and Sea-Wave Properties. J. Earthq. Eng., 26(14), 7222–7244.
665   https://doi.org/10.1080/13632469.2021.1961936

666 IEC 61400-3-1. (2019). Wind energy generation systems Part 3-1:Design requirements
667   for fixed offshore wind turbines.

668 Jonkman, B. J. and Buhl, M. L. (2006). TurbSim User's Guide. Tech. Rep., 500, 39797.

669 Jonkman, J., Butterfield, S., Musial, W. and Scott, G. (2009). Definition of a 5-MW
670   Reference Wind Turbine for Offshore System Development (NREL/TP-500-
671   38060, 947422; p. NREL/TP-500-38060, 947422).

672 Jung, S., Kim, S.-R., Patil, A. and Hung, L. C. (2015). Effect of monopile foundation
673   modeling on the structural response of a 5-MW offshore wind turbine tower.
674   Ocean Eng., 109, 479–488.

675 Klaus, H., Dirk, J. O. and Peter, M. (1973). Measurements of wind-wave growth and
676   swell decay during the joint North Sea wave project (JONSWAP).

677 Lackner, M. A. and Rotea, M. A. (2011a). Passive structural control of offshore wind
678   turbines. Wind Energy, 14(3), 373–388. https://doi.org/10.1002/we.426

679 Lackner, M. A. and Rotea, M. A. (2011b). Structural control of floating wind turbines.
680   Mechatronics, 21(4), 704–719. https://doi.org/10.1016/j.mechatron-
681   ics.2010.11.007

682 Liang, F., Chen, H. and Jia, Y. (2018). Quasi-static p-y hysteresis loop for cyclic lateral
683   response of pile foundations in offshore platforms. Ocean Eng., 148, 62–74.
684   https://doi.org/10.1016/j.oceaneng.2017.11.024

685 Lu, D., Wang, W. and Li, X. (2023). Experimental study of structural vibration control
686   of 10-MW jacket offshore wind turbines using tuned mass damper under wind
687   and wave loads. Ocean Eng., 288, 116015.
688   https://doi.org/10.1016/j.oceaneng.2023.116015

689 Ma, H. and Chen, C. (2021). Scour protection assessment of monopile foundation de-
690   sign for offshore wind turbines. Ocean Eng., 231, 109083.
691   https://doi.org/10.1016/j.oceaneng.2021.109083

692   Mayall, R. O., McAdam, R. A., Byrne, B. W., Burd, H. J., Sheil, B. B., Cassie, P. and
693   Whitehouse, R. J. S. (2018). Experimental modelling of the effects of scour on
694   offshore wind turbine monopile foundations. In A. McNamara, S. Divall, R.
695   Goodey, N. Taylor, S. Stallebrass, and J. Panchal (Eds.), PHYSICAL MODEL-
696   LING IN GEOTECHNICS, VOL 1 (pp. 725–730). Int Soc Soil Mech & Ge-
697   otechn Engn, Tech Comm 104 Phys Modelling Geotechn; Active Dynam;
698   Tekscan.

699   Nakagawa, H. and Suzuki, K. (1976). Local Scour Around Bridge Pier in Tidal Current.
700   Coast. Eng. Jpn., 19(1), 89–100.
701   https://doi.org/10.1080/05785634.1976.11924219

702   Pedersen, D. M. and Askheim, H. (2021). Implementation of seismic soil-structure in-
703   teraction in OpenFAST and application to a 10MW offshore wind turbine on
704   jacket structure. Norwegian University.

705   Pelayo, F., Skafte, A., Aenlle, M. L. and Brincker, R. (2015). Modal Analysis Based
706   Stress Estimation for Structural Elements Subjected to Operational Dynamic
707   Loadings. Exp. Mech., 55(9), 1791–1802. https://doi.org/10.1007/s11340-015-
708   0073-6

709   Rezaei, R. (2017). Fatigue Sensitivity of Monopile-supported Offshore Wind Turbines.
710   University College London.

711   Rezaei, R., Duffour, P. and Fromme, P. (2018). Scour influence on the fatigue life of
712   operational monopile-supported offshore wind turbines. Wind Energy, 21(9),
713   683–696. https://doi.org/10.1002/we.2187

714   Rudolph, D., Bos, K. J., Luijendijk, A. P. and Rietema, K. (2016). Scour around off-
715   shore structures-analysis of field measurements.

716   Shahmohammadi, A. and Shabakhty, N. (2020). Pile Apparent Fixity Length Estima-
717   tion for the Jacket-type Offshore Wind Turbines under Lateral Loads Applica-
718   ble to Fatigue Analysis. Int. J. Coast. Offshore Eng., 3(4), 25–33.
719   https://doi.org/10.29252/ijcoe.3.4.25

720   Shirzadeh, R., Devriendt, C., Bidakhvidi, M. A. and Guillaume, P. (2013). Experi-
721   mental and computational damping estimation of an offshore wind turbine on a
722   monopile foundation. J. Wind Eng. Ind. Aerodyn., 120, 96–106.
723   https://doi.org/10.1016/j.jweia.2013.07.004

724   Song, J. and Achmus, M. (2023). Cyclic overlay model of $p - y$ curves for laterally
725   loaded monopiles in cohesionless soil. Wind Energy Sci., 8(3), 327–339.
726   https://doi.org/10.5194/wes-8-327-2023

727   Sørensen, P. H. S. and Ibsen, L. B. (2013). Assessment of foundation design for off-
728   shore monopiles unprotected against scour. Ocean Eng., 63, 17–25.

729   Stieng, L. E. S. and Muskulus, M. (2020). Reliability-based design optimization of off-
730   shore wind turbine support structures using analytical sensitivities and factor-
731   ized uncertainty modeling. Wind Energy Sci., 5(1), 171–198.
732   https://doi.org/10.5194/wes-5-171-2020

733   Tang, Z., Melville, B., Shamseldin, A., Guan, D., Singhal, N. and Yao, Z. (2023). Ex-
734   perimental study of collar protection for local scour reduction around offshore
735   wind turbine monopile foundations. Coast. Eng., 183, 104324.
736   https://doi.org/10.1016/j.coastaleng.2023.104324

van der Tempel, J. (2006). Design of support structures for offshore wind turbines. Technische Universiteit Delft.

Velarde, J., Kramhøft, C., Sørensen, J. D. and Zorzi, G. (2020). Fatigue reliability of large monopiles for offshore wind turbines. Int. J. Fatigue, 134, 105487. https://doi.org/10.1016/j.ijfatigue.2020.105487

Wang, G., Xu, S., Zhang, Q. and Zhang, J. (2023). An experimental study of the local scour protection methods around the monopile foundation of offshore wind turbines. Ocean Eng., 273, 113957. https://doi.org/10.1016/j.oceaneng.2023.113957

Wang, L., Zhou, W., Guo, Z. and Rui, S. (2020). Frequency change and accumulated inclination of offshore wind turbine jacket structure with piles in sand under cyclic loadings. Ocean Eng., 217, 108045. https://doi.org/10.1016/j.oceaneng.2020.108045

Wang, X., Zeng, X., Li, X. and Li, J. (2019). Investigation on offshore wind turbine with an innovative hybrid monopile foundation: An experimental based study. Renew. Energy, 132, 129–141. https://doi.org/10.1016/j.renene.2018.07.127

Zdravković, L., Taborda, D., Potts, D., Jardine, R., Sideri, M., Schroeder, F., Byrne, B., McAdam, R., Burd, H., Houlsby, G., et al. (2015). Numerical modelling of large diameter piles under lateral loading for offshore wind applications. Front. Offshore Geotech. III, 759–764.

Zhang, F., Chen, X., Feng, T., Wang, Y., Liu, X. and Liu, X. (2022). Experimental study of grouting protection against local scouring of monopile foundations for offshore wind turbines. Ocean Eng., 258, 111798. https://doi.org/10.1016/j.oceaneng.2022.111798

Zhang, F., Chen, X., Yan, J. and Gao, X. (2023). Countermeasures for local scour around offshore wind turbine monopile foundations: A review. Appl. Ocean Res., 141, 103764. https://doi.org/10.1016/j.apor.2023.103764

Zhang, H., Liang, F. and Zheng, H. (2021). Dynamic impedance of monopiles for offshore wind turbines considering scour-hole dimensions. Appl. Ocean Res., 107, 102493. https://doi.org/10.1016/j.apor.2020.102493

Zhang, R., Zhao, Z. and Dai, K. (2019). Seismic response mitigation of a wind turbine tower using a tuned parallel inerter mass system. Eng. Struct., 180, 29–39. https://doi.org/10.1016/j.engstruct.2018.11.020